Optics Letters

Scan-less 3D microscopy based on spatiotemporal encoding on a single-cavity dual-comb laser

Wanping Lu,[1,†] Zhiwei Zhu,[1,†] Benjamin Willenberg,[2] Justinas Pupeikis,[2] Christopher R. Phillips,[2] Ursula Keller,[2] and Shih-chi Chen[1,3,*]

[1]Department of Mechanical and Automation Engineering, The Chinese University of Hong Kong, Shatin, N.T., Hong Kong SAR, China
[2]Department of Physics, Institute for Quantum Electronics, ETH Zurich, Auguste-Piccard-Hof 1, 8093 Zurich, Switzerland
[3]Hong Kong Centre for Cerebro-Cardiovascular Health Engineering (COCHE), Hong Kong Science Park, Shatin, Hong Kong SAR, China
[†]These authors contributed equally to this work.
[*]scchen@mae.cuhk.edu.hk

Received 6 October 2023; revised 27 February 2024; accepted 27 February 2024; posted 29 February 2024; published 25 March 2024

Dual-comb microscopy enables high-speed and high-precision optical sampling by simultaneously extracting both amplitude and phase information from the interference signals with frequency division multiplexing. In this Letter, we introduce a spatiotemporal encoding approach for dual-comb microscopy that overcomes previous limitations such as mechanical scanning, low sampling efficiency, and system complexity. By employing free-space angular-chirp-enhanced delay (FACED) and a low-noise single-cavity dual-comb laser, we achieve scan-less 3D imaging with nanometer precision and a 3D distance-imaging rate of 330 Hz, restricted only by the repetition rate difference of the dual-comb laser. Specifically, the FACED unit linearly arranges the laser beam into an array. A grating subsequently disperses this array transversely into lines, facilitating ultrafast spectroscopic applications that are 1–2 orders of magnitude quicker than traditional dual-comb methods. This spatiotemporal encoding also eases the stringent conditions on various dual-comb laser parameters, such as repetition rates, coherence, and stability. Through carefully designed experiments, we demonstrate that our scan-less system can measure 3D profiles of microfabricated structures at a rate of 7 million pixels per second. Our method significantly enhances measurement speed while maintaining high precision, using a compact light source. This advancement has the potential for broad applications, including phase imaging, surface topography, distance ranging, and spectroscopy.

https://doi.org/10.1364/OL.507661

Advancement in 3D imaging techniques has driven the rapid development of biomedical sciences and materials research. In the past few decades, a variety of imaging techniques have been developed to visualize two-dimensional (2D) and three-dimensional (3D) specimens with improved resolution and rate, such as confocal microscopy [1], optical coherence tomography [2], structured illumination microscopy [3], and light-sheet microscopy [4]. One important application of microscopy techniques is to perform distance imaging, which covers many important engineering applications, such as 3D surface profiling, defect detection, and absolute distance measurement. Traditionally, 3D surface mapping with distance measurements is achieved by mechanically scanning the laser focus over the surface of a sample with a confocal microscopy approach, which has limited speed and accuracy. Recently, spatial light modulators such as digital micromirror devices [5,6] have been adopted to achieve fast 2D and 3D scanning using single or multiple laser foci with improved spatial repeatability and high stability.

An alternative method for rapid 3D surface profiling utilizes spectral encoding of the specimen's geometry via a dual-comb source. The optical frequency comb (OFC) has proven to be an effective light source for this purpose, offering a multitude of frequency channels for precise measurements [7]. Dual-comb interferometry [8–10] serves as a robust mechanism for decoding time, amplitude and phase from OFC, enabling high-speed depth information extraction using a single-pixel photodetector. For example, one-dimension (1D) spectral encoding [11], combined with dual-comb interferometry, has significantly accelerated 3D surface profiling. In this context, the time-of-flight (TOF) method [8] has been employed to accurately reconstruct the depth information [9]. For scan-less imaging, 2D spectral encoding can be achieved using a virtually imaged phased array (VIPA) in conjunction with a diffraction grating oriented in the orthogonal direction [12]. This method has been implemented in dual-comb systems and has reported a phase imaging resolution of 0.028 rad [10]. While multi-channel scanning can effectively eliminate the need for mechanical scanning, it introduces system complexity, particularly the requirement for a fully stabilized dual-comb source, and limits flexibility. A compact system capable of capturing high-resolution 3D profiles in a single measurement has yet to be developed.

In this Letter, we introduce a 3D scan-less dual-comb microscopy that utilizes spatiotemporal encoding and a custom single-cavity dual-comb laser. The method achieves spatiotemporal encoding by simultaneously implementing time-to-space and wavelength-to-space conversion in two orthogonal directions. Our dual-comb system reaches an imaging speed of 330 Hz covering an area of 679×32 pixels, which results in an acquisition speed of approximately 7 million pixels/second.

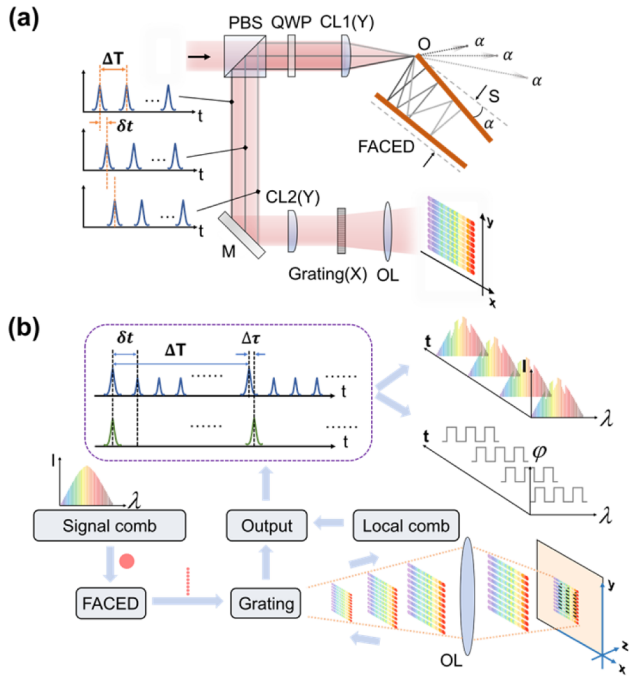

Fig. 1. (a) Principle of spatiotemporal 2D encoding; (b) spatiotemporal encoding for scan-less 3D imaging via a dual-comb system.

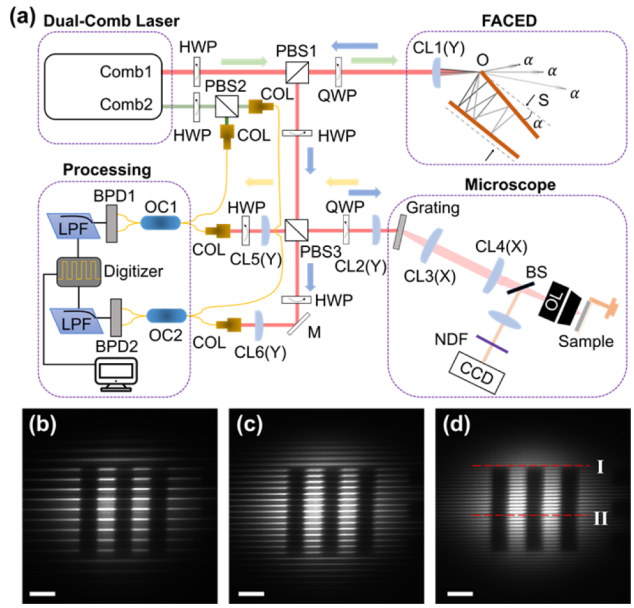

Fig. 2. (a) Experimental setup for scan-less dual-comb microscopy. HWP, half-wave plate; PBS 1–3, polarization beam splitters; QWP, quarter-wave plate; CL 1–6, cylindrical lenses; BS, beam splitter; OL, objective; NDF, neutral density filter; M, mirror; COL, collimator; OC, optical coupler; BPD, balanced photodetector; and LPF, low-pass filter. (b)–(d) Images of the 2D line-array with 15 lines, 25 lines, and 40 lines, respectively. (Scale bar = 50 μm.)

The system also offers a depth resolution of 6.86 nm for scan-less 3D imaging.

Figure 1(a) illustrates the fundamental concept of the spatiotemporal encoding. Initially an OFC undergoes time-to-space conversion with a free-space angular-chirp-enhanced delay (FACED) setup [13]. The FACED setup utilizes a misalignment angle α between a pair of mirrors with a distance S to generate a vertically oriented array of discrete points along the y axis. This beam array, which has a discrete pulse front tilt, is retroreflected to the entrance O and transferred to the image plane via the cylindrical lens CL2(Y) and objective lens (OL). Therefore, the FACED setup provides an approximately equal time delay δt ($\approx 2S/c$) between the neighboring spots on the y axis. In order to enable 2D scan-less spatiotemporal encoding, a diffraction grating disperses the spectrum along the horizontal direction (x axis). We thereby obtain a 2D pattern at the focal plane of the objective lens (OL) consisting of a frequency-to-space mapping along x and a time-to-space mapping along y. This configuration is functionally equivalent to a vertical array of spatially chirped OFC sources.

Figure 1(b) depicts the process wherein the information-encoded signal combs interact with the local comb to achieve dual-comb interferometry. In the time domain, many information-encoded new pulses, each separated by a time interval of δt, are contained within one period (ΔT) of the original signal comb. The local comb, in contrast, has a slightly different period denoted as $\Delta T + \Delta\tau$. Therefore, interferograms (IGMs) of all new pulses can be obtained within a single beat period. This is a significant improvement over traditional dual-comb line-scanning systems, which are limited by beat periods for their scan rates.

Note the spatiotemporal encoding technique has the potential to accelerate the update rate of dual-comb imaging systems to megahertz range with a faster light source [14]. This approach also offers a new paradigm for 2D spectral encoding, providing a simpler design and less stringent light source requirements compared to the VIPA method. By segmenting and decoding the IGMs in different time channels, both amplitude and phase spectra for each line can be retrieved, enabling the reconstruction of 3D sample images.

Figure 2(a) outlines the experimental setup of the scan-less dual-comb microscopy with spatiotemporal encoding. The light source is a custom-built dual-comb laser [15] that uses a single-cavity to generate simultaneous mode-locking for two combs (i.e., Comb 1 and Comb 2) with a pulse width of sub-140 fs, repetition rates around 80 MHz, a center wavelength around 1052 nm, and an average power of 2 W per comb. In addition, the relative timing jitter was measured to be only 2.2 fs (20 Hz, 100 kHz) in free-running operation. Piezo-actuated mirrors are integrated within the laser cavity for closed-loop control of the repetition rates and their difference. In following experiments, Comb 2 was stabilized at an 80-MHz repetition rate, with a rate difference set to 330 Hz (i.e., $\Delta\tau \approx 51$ fs).

Our system shows the optical pathway for Comb 1, designated as the signal comb. Initially, Comb 1 passes through a half-wave plate (HWP), a polarizing beam splitter (PBS1), and a quarter-wave plate (QWP) to enter the FACED system. This unit consists of a cylindrical lens (CL1(Y)) and a pair of high-reflectivity dielectric multilayer mirrors. The beams leaving the FACED system pass back through the QWP and are reflected by PBS1 toward PBS3. A portion of Comb 1 is transmitted by PBS3 and acts as the reference beams, while the remaining light is reflected by PBS3 and acts as the signal beams. The reference beams are combined with a portion of Comb 2 by a 50:50 fiber optical coupler (OC2). The signal beams propagate to the microscope module: in the y axis, the discrete pulse front tilt is transferred

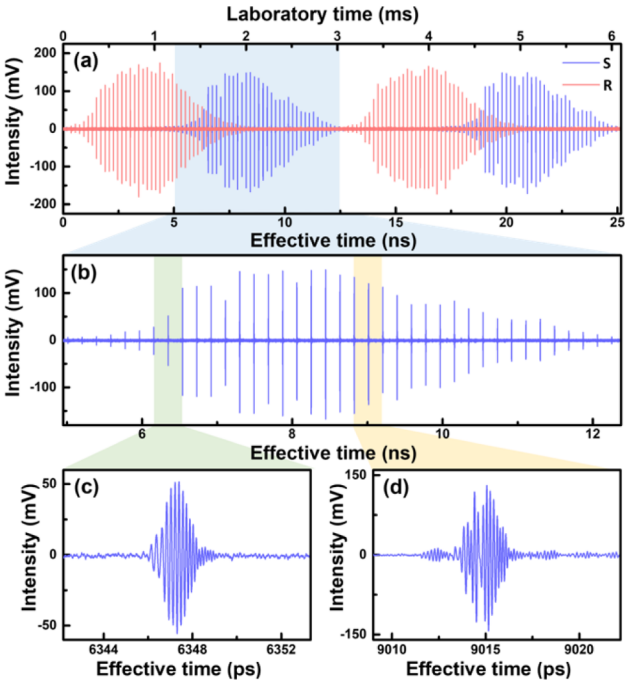

Fig. 3. (a) IGMs of the signal comb (blue) and reference comb (red). (b) Zoom-in view of one group of signal combs (c) and (d) Zoom-in IGMs of line I (close to the resolution target) and line II (across the target) in Fig. 2(d).

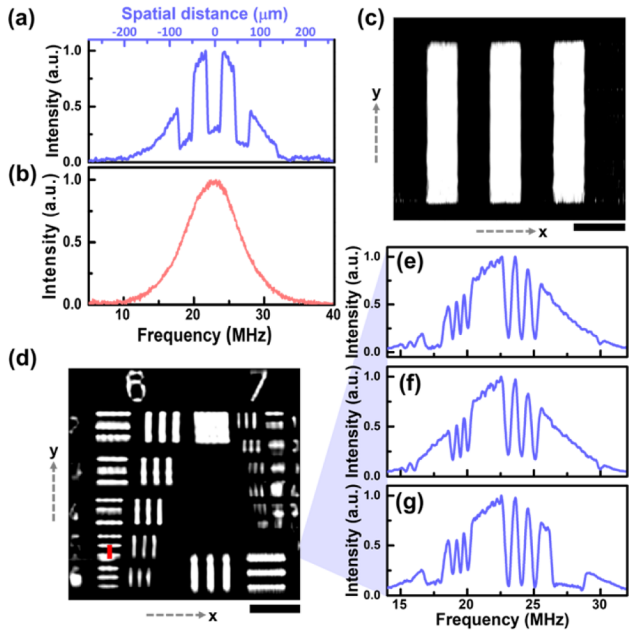

Fig. 4. Amplitude imaging. (a) Amplitude spectrum of the image-encoded line and (b) the corresponding reference amplitude spectrum. (c) Amplitude image of the resolution target in Fig. 2(d). (d) Amplitude image of Group 6 and 7 bars on the resolution target. (e)–(g) Signal amplitude spectra of three adjacent lines, labeled by the red vertical line in (d). (Scale bar = 50 μm.)

to the image plane via lenses CL2(Y) and OL. In the x axis, a spatial chirp is realized by the grating and lenses CL3(X), CL4(X), and OL. Subsequently, a 2D line-array forms at the focal plane to encode the sample.

The resulting images are relayed to a CCD camera via a beam splitter (BS), a lens, and a neutral density filter (NDF) for real-time monitoring. Notably, the line density projected onto the sample can be adjusted by varying the spacing between adjacent lines. This is demonstrated in Figs. 2(b)–2(d), which show 2D line-arrays with different line densities (i.e., 15, 25, and 40 lines) projected onto a resolution target.

The signals reflected from the microscope module are first routed through PBS3 and then directed into the processing module via optical coupler 1 (OC1) with a 50% coupling ratio. Subsequently, the signal and the reference combs from OC1 and OC2 are combined and interfered with Comb 2. The resulting IGMs from both OC1 and OC2 are captured by balanced photodetectors (BPDs) and then filtered through 40-MHz low-pass filters (LPFs). Finally, these filtered signals are digitized using a dual-channel data acquisition card for subsequent post-processing. For comprehensive system details, please refer to Supplement 1.

Figure 3(a) displays time-domain data for signal IGMs in blue and reference IGMs in red, acquired via the dual-comb microscope. These correspond to the image-encoded line-array depicted in Fig. 2(d). The IGMs were sampled at a rate of 500 M samples/s, resulting in approximately 40 lines of varied intensities as shown in Fig. 3(b). The distinct features between Figs. 3(c) and 3(d), representing IGMs for line I and line II in Fig. 2(d) respectively, are evident.

The amplitude and phase images for each line can be reconstructed by Fourier transforming the IGMs into the frequency domain. The temporal width of the IGMs is determined by the time delay (δt) between adjacent lines (in Fig. 2(d)), which is set by the FACED unit. Note that δt should be carefully selected to ensure all FACED-generated pulses are within ΔT (i.e., 12.5 ns) to avoid temporal aliasing. In this system, δt was set as 189.75 ps (corresponding to $S = 28.46$ mm as shown in Fig. 1), which translates to a radio frequency resolution of 21.74 kHz.

Figures 4(a) and 4(b) display the amplitude spectrum of line II (corresponding to Fig. 3(d)) and its related reference comb (depicted in red in Fig. 3(a)), both captured within a beat period of 3 ms. The field of view (FOV) in the horizontal direction (x axis) is 230 μm, which is determined by the spectral range (i.e., 283.08–286.66 THz). Here, each line contains 3.58 THz · (330 Hz / 80 MHz) / 21.74 kHz = 679 effective pixels.

We then obtain the wavelength-to-space mapping by extracting the spectral differences between the two spectra, followed by analyzing the spectra of all lines. As such, based on the intensity of IGMs, 32 lines within an FOV of 200 μm in the vertical direction (y axis) are selected to reconstruct the amplitude image. Figure 4(c) presents the restored amplitude image of the UASF-1951 resolution target (Element 1 of Group 4) at a frame rate of 330 Hz.

To characterize the lateral resolution of the system, we imaged the resolution target with different magnifications. Figure 4(d) shows the reconstructed amplitude image (Group 6 and Group 7), indicating resolutions of 5.52 μm (Element 4, Group 7) and 8.76 μm (Element 6 of Group 6) along the x and y axes, respectively. Note that lower y axis resolution results from setting line distances above the minimum width to avoid cross talk, as shown in Figs. 4(e)–4(g). While reducing the line distance can improve resolution, it may reduce signal-to-noise ratio, particularly at the vertical edges of the FOV. Further discussion on resolution is provided in Supplement 1.

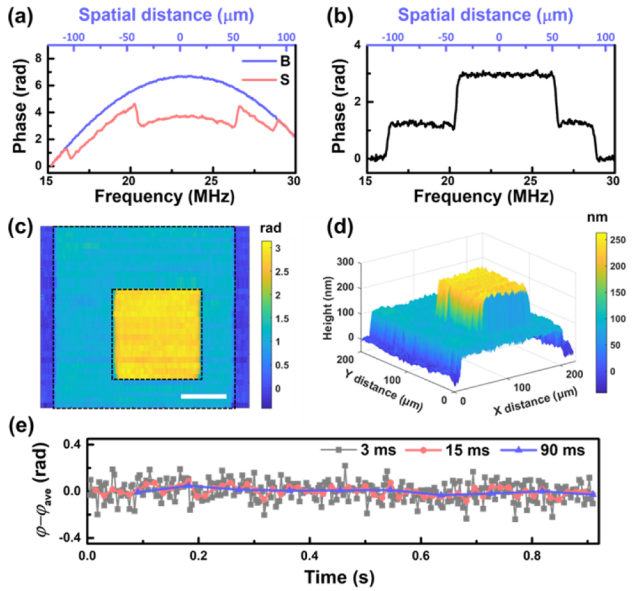

Fig. 5. Phase imaging of a 3D sample. (a) Normalized phase spectra of the sample (red line) and background (blue line) lines. (b) Phase difference between the two lines in (a). (c) Phase image and (d) the corresponding 3D surface profile of the sample. (Scale bar = 50 μm.) (e) Phase resolution.

To evaluate the 3D imaging capability, we performed scanless imaging on a silver-coated two-step structure, which was fabricated via photolithography processes. In the experiment, the 2D line-array was set up as shown in Fig. 2(d). We then sequentially imaged the sample and its background, where representative sample (S) and background (B) lines are presented in Fig. 5(a). Next, the phase profile, shown in Fig. 5(b), was calculated based on Eq. (1), where the reference combs were used for correction:

$$\varphi = (\varphi_{S,sig} - \varphi_{B,sig}) - (\varphi_{S,ref} - \varphi_{B,ref}), \quad (1)$$

where $\varphi_{S,sig}$ and $\varphi_{S,ref}$ are the phase of the signal and the corresponding reference combs, respectively, while $\varphi_{B,sig}$ and $\varphi_{B,ref}$ are the phase for the background surface. In Fig. 5(b), the two-step structure in reference to the background surface can be clearly observed. By combining the relative phase spectra of 32 lines along the y axis, a phase image of the sample can be reconstructed, as shown in Fig. 5(c). According to the measurement principle, the detectable phase change is $\pm\pi$. Thus, the relative height of each pixel and the axial detection range can be calculated by

$$h(x, y) = \lambda \times \varphi(x, y)/(4\pi), \quad (2)$$

where λ is the central wavelength (i.e., 1052 nm). Based on Eq. (2), a 3D image of the sample can be reconstructed, as shown in Fig. 5(d). The axial (or depth) resolution of the image can be found by calculating the phase variation of one pixel with different averaging time. The results are presented in Fig. 5(e), where the standard deviations of phase values are 0.082 rad for 3 ms, 0.041 rad for 15 ms, and 0.024 rad for 90 ms. These correspond to a depth resolution of 6.86, 3.43, and 2.01 nm, respectively. Comparing with VIPA [10], our system also allows for absolute distance measurement of each pixel based on the TOF method [9], which can extend the measurement range to a millimeter level. See Supplement 1 for more absolute distance ranging results from our dual-comb microscopy.

In summary, we have introduced, to our knowledge, a novel dual-comb microscopy approach utilizing a spatiotemporal encoding technique. By integrating time-to-space conversion (via FACED) with wavelength-to-space conversion, we have developed a 2D spectral encoding method for scan-less 3D microscopy. Employing a custom-built, low-noise, single-cavity dual-comb laser, we achieved a 3D imaging rate of 330 Hz over a field of view of 230 μm × 200 μm, covering 679 × 32 pixels. Experiments using resolution targets and custom-fabricated 3D samples confirmed high-precision 3D surface profiling via phase imaging with a depth resolution of 6.86 nm. These results indicate substantial potential to increase the speed of dual-comb measurements by increasing the duty ratio by more than 10 times while also providing spatially resolved imaging capabilities with ultrafast self-scanning.

Funding. Research Grants Council; General Research Fund (14209421); Innovation and Technology Commission (ITS/213/22FP); InnoHK Centre (COCHE-1.5); Swiss National Science Foundation (40B2-0_180933).

Disclosures. The authors declare no conflicts of interest.

Data availability. Data underlying the results presented in this paper are not publicly available at this time but may be obtained from the authors upon reasonable request.

Supplemental document. See Supplement 1 for supporting content.

REFERENCES

1. P. Davidovits and M. D. Egger, Nature **244**, 366 (1973).
2. D. Huang, E. A. Swanson, C. P. Lin, *et al.*, Science **254**, 1178 (1991).
3. M. G. Gustafsson, J. Microsc. **198**, 82 (2000).
4. J. Huisken, J. Swoger, F. Del Bene, *et al.*, Science **305**, 1007 (2004).
5. Q. Geng, C. Gu, J. Cheng, *et al.*, Optica **4**, 674 (2017).
6. Q. Geng, D. Wang, P. Chen, *et al.*, Nat. Commun. **10**, 2179 (2019).
7. T. Udem, R. Holzwarth, and T. W. Hänsch, Nature **416**, 233 (2002).
8. I. Coddington, W. C. Swann, L. Nenadovic, *et al.*, Nat. Photonics **3**, 351 (2009).
9. C. Wang, Z. Deng, C. Gu, *et al.*, Opt. Lett. **43**, 1606 (2018).
10. E. Hase, T. Minamikawa, T. Mizuno, *et al.*, Optica **5**, 634 (2018).
11. D. Yelin, I. Rizvi, W. M. White, *et al.*, Nature **443**, 765 (2006).
12. K. Goda, K. Tsia, and B. Jalali, Nature **458**, 1145 (2009).
13. J. Wu, Y. Xu, J. Xu, *et al.*, Light: Sci. Appl. **6**, e16196 (2016).
14. V. Durán, S. Tainta, and V. Torres, Opt. Express **23**, 30557 (2015).
15. J. Pupeikis, B. Willenberg, S. L. Camenzind, *et al.*, Optica **9**, 713 (2022).